Modeling the Electromagnetic Structure of Deuteron Using Low Energy Nuclear Theory

Sarah Heller, Alex Gnech

https://doi.org/10.15788/739245823

Modeling the Electromagnetic Structure of Deuteron Using Low Energy Nuclear Theory

[1)]Montana State University [2)]Old Dominion University [3)]Thomas Jefferson National Accelerator Facility

By Sarah Heller[1], Alex Gnech[2,3]

Abstract

Deuteron, the simplest possible nucleus consisting of a proton and neutron, is often used as a target in electro-scattering experiments, where a beam of electrons collides with a stationary deuteron sample. To calculate the interaction between the deuteron and electron, it is necessary to have a working model of the deuteron's nuclear potential and the resulting wave function. In cases where the internal substructure of the nucleons is negligible, such as with elastic scattering, a low energy theory may be used to describe the deuteron. In this regime, the nuclear interaction binding the proton and neutron contains One Pion Exchange potentials (V_OPE), the tensor operator (Š12), and spin/isospin coupling terms. The goal of this project was to calculate the deuteron wave function and physical electromagnetic observables using this low-energy nuclear potential starting from the three-dimensional Schrodinger equation. This was accomplished using both analytical and computational methods. The matrix elements for the spin, isospin, and angular components were derived analytically using Wigner coefficients and angular momentum coupling techniques. The radial component matrix elements were solved computationally using Gaussian-Laguerre quadrature integration and matrix linear algebra. The resulting observables, including the ground-state binding energy (-2.2245 MeV), root mean square radius (1.908 fm), and magnetic moment (0.854 μN), all align with experimental measurements. These results indicate that the interaction potential and low-energy assumptions used are valid and model the deuteron accurately. Electron-deuteron elastic scattering experiments, such as those at Jefferson National Lab, could make use of this model to calculate the theoretical cross-sections to compare to their experimental data. The model could also be extended to experiments outside of Jefferson Lab to compute cross-sections for neutrino-deuteron elastic scattering.

The deuteron nucleus is made of a single proton and a neutron bound together and is the 2nd lightest nucleus beyond a single proton. We are motivated to study the binding interaction and resulting deuteron wave function as the first step in understanding more complex nuclei. Furthermore, understanding how the two constituent particles (the proton and neutron) bind together is necessary information in determining how other external particles interact with the deuteron as a whole. The simplest type of external interaction is

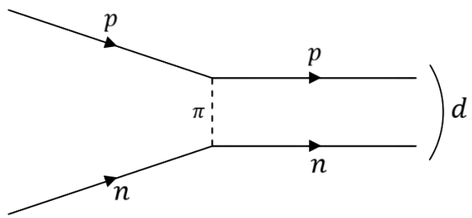

Figure 2: Feynman diagram of one pion exchange between a neutron and proton, forming a deuteron nucleus.

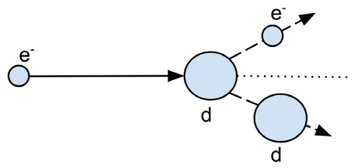

Figure 1: Electron-deuteron elastic scattering kinematics diagram.

elastic electro-scattering, where a beam of electrons is scattered off a stationary deuteron sample. Elastic scattering occurs when the total kinetic energy is conserved, and the internal structure of each particle (and thus its identity) is maintained, as shown in Fig. 1. Such interactions are frequently created at Jefferson Laboratory and other collider facilities. Thus, to predict how electrons will interact with the stationary deuteron targets in experimental settings, we must first model the deuteron and its wave function.

When modeling elastic scattering off a deuteron or a deuteron V_{OPE} by itself (with no external interaction), we can use a first-order interaction potential that does not consider the internal quark structure of the proton or neutron. In this low energy regime, the dominating interaction that holds the deuteron together is the One Pion Exchange Potential (Š12), depicted in Fig. 2.(Š12), The full nuclear interaction potential as given by van Kolck1 reads,

$$\hat{V} = V_{CT}(r)\left(\frac{3+\sigma_1\cdot\sigma_2}{4}\right)\left(\frac{1-\tau_1\cdot\tau_2}{4}\right)\delta_{L,0} + \left(V_{OPE}^{(1)}(r)\hat{S}_{12} + V_{OPE}^{(2)}(r)\sigma_1\cdot\sigma_2\right)(\tau_1\cdot\tau_2)$$

$$\hat{S}_{12} = 3(\sigma_1\cdot\hat{r})(\sigma_2\cdot\hat{r}) - \sigma_1\cdot\sigma_2$$

Where $\hat{\sigma}$ is the operator that acts on the spin and $\hat{\tau}$ is the operator that acts on isospin. From previous literature (Piarulli et al) we define the exact contact potential V_{CT} and one-pion-exchange potentials as follows:

$$V_{CT}(r) = \frac{C_S}{\pi^{\frac{3}{2}}R_S^3}e^{-\left(\frac{r}{R_S}\right)^2}$$

$$V_{OPE}^{(1)}(r) = \frac{g_A^2 m_\pi^3}{12\pi F_\pi^2}\frac{e^{-m_\pi r}}{m_\pi r}\left(1+\frac{3}{m_\pi r}+\frac{3}{(m_\pi r)^2}\right)C_{R_L}(r)$$

$$V_{OPE}^{(2)}(r) = \frac{g_A^2 m_\pi^3}{12\pi F_\pi^2}\frac{e^{-m_\pi r}}{m_\pi r}\,C_{R_L}(r)$$

where $R_S = 0.7$ fm and $C_S = -1.2565$ fm^2 is a constant fixed to reproduce the binding energy of the deuteron. R_S plays the role of a cut-off.

Additionally, to handle singularities at short distances (such as dividing by factors of r), a regularizing function is introduced to smooth the potential;

$$C_{R_L}(r) = 1 - \frac{1}{\left(\frac{r}{R_L}\right)^6 e^{\left(\frac{r-R_L}{a_L}\right)} + 1}$$

is the regularizing function with $R_L = 1.0$fm and $a_L = \frac{R_L}{2}$. The other constants are the nucleon axial coupling $g_A = 1.29$, the pion decay constant $F_\pi = 184.80$ MeV and the mean mass of the pion $m_\pi = 138.04$ MeV.

The goal of this project is to model the deuteron using the described low energy interaction potential, and finding the ground-state wave function, binding energy, and other electromagnetic observables. Section 2A constructs the wavefunction. Section 2B solves the Schrödinger equation as far as possible using analytical methods. Section 2C computationally solves for the remaining components and calculates several physical observables of the deuteron. Finally, sections 3 and 4 present the final results and discuss their significance.

Methods

Constructing the Wave FunctionWe construct the deuteron wave function as the tensor product of the radial, angular, spin, and isospin components. Experimental results show that the deuteron has positive parity and a total angular momentum of $J = 1$, constraining the possible quantum numbers. The wave function then f_L the form shown below, with only the radial functions remaining unknown.

$$\psi_{1J_z}(r) = \sum_{L=0,2} f_L(r)[Y_L(\hat{r})\mathcal{X}_{S=1}]_{1J_z}\,\mathcal{X}_{\mathcal{T}=0,\mathcal{T}_z=0}$$

The equation above shows that the total wave function of the deuteron is the sum of the S and D waves, where the S wave has a total orbital angular momentum of 0 (L=0) and the D wave has a total orbital angular momentum of 2 (L=2). We know the angular, spin, and isospin components exactly: the Y_L's are the typical spherical harmonics, the X_S's are the coupled spins, and the X_T's are the coupled isospins given by,

$$\mathcal{X}_{SS_z} = [s_1 s_2]_{SS_z} = \sum_{s_{1z},s_{2z}} \langle 1/2\, s_{1z}\, 1/2\, s_{2z}|S\, S_z\rangle\, |1/2\, s_{1z}\rangle\, |1/2\, s_{2z}\rangle$$

and, analogously

$$\mathcal{X}_{\mathcal{T}\mathcal{T}_z} = [t_1 t_2]_{TT_z} = \sum_{t_{1z},t_{2z}} \langle 1/2\, t_{1z}\, 1/2\, t_{2z}|T\, T_z\rangle\, |1/2\, t_{1z}\rangle\, |1/2\, t_{2z}\rangle$$

where the first term in the summation is a Clebch-Gordan coefficient.

To solve for the unknown radial component of the wave function, we expand the f_L radial functions onto the 2nd order Laguerre polynomial basis ($L^{(2)}$) along with a normalization term and a negative exponential that accounts for the decay behavior of the nuclear interaction (i.e. the deuteron's wave function going to zero as the distance separating the two particles grows and the wave function going to zero as the two particles approach the same location). This leaves

the expansions coefficients ($\mathbf{c_l}$) as the only unknown parts of the wave function that must be solved within the Schrödinger eigenvalue equation.

$$f_L(r) = \sum_l c_l^L \, g_l(r)$$

$$g_l(r) = N_l L_l^{(2)}(\gamma r) e^{-\frac{\gamma r}{2}}$$

$$N_l = \gamma^{3/2} \sqrt{\frac{l!}{(l+2)!}}$$

Analytical Solution

To solve the 3D Schrödinger equation, we apply the variational principle to find the ground state wave function and energy by solving the associated eigenvalue equation.

$$\frac{\langle \Psi(r) | \hat{H} | \Psi(r) \rangle}{\langle \Psi(r) | \Psi(r) \rangle} \geq E_{ground}$$

In this way, we find the minimum ground state binding energy and the corresponding wave function expansion coefficients. Thus, it is necessary to find all of the Hamiltonian matrix elements, including the values contributed by both the kinetic and potential energy terms. Applying the nuclear potential to the wave function within the Hamiltonian matrix, we find non-zero matrix elements that can be computed analytically: pure spin/isospin elements and the tensor operator element.

$$\langle \mathcal{X}_\mathcal{T} \mid (\tau_1 \cdot \tau_2) \mid \mathcal{X}_\mathcal{T} \rangle$$

$$\langle \mathcal{X}_\mathcal{S} \mid (\sigma_1 \cdot \sigma_2) \mid \mathcal{X}_\mathcal{S} \rangle$$

$$\langle [Y_L(\hat{r}) \mathcal{X}_\mathcal{S}] \mid \hat{S}_{12} \mid [Y_L(\hat{r}) \mathcal{X}_\mathcal{S}] \rangle$$

To solve these elements, we expand and rearrange the spinors, spherical harmonics, and operators using Clebsch-Gordan and Wigner coefficients (expansion coefficients used in the coupling of 2+ angular momenta). Given states of definite spin and orbital angular momentum, these terms reduce to constants and coefficients in the remaining radial equation.

Once all three spin, isospin, and tensor operator matrix elements are calculated, their values can be plugged back into the Hamiltonian matrix. If we explicitly expand the wave function, we are left with the following radial functions. These are coupled differential equations as they both contain the f_0 and f_2 terms.

$$Ef_0(r) = -\frac{1}{2\mu}\frac{1}{r^2}\frac{\partial}{\partial r}\left(r^2 \frac{\partial f_0(r)}{\partial r}\right) + V_{00}(r) f_0(r) + V_{02}(r) f_2(r)$$

$$Ef_2(r) = -\frac{1}{2\mu}\left(\frac{1}{r^2}\frac{\partial}{\partial r}\left(r^2 \frac{\partial f_2(r)}{\partial r}\right) + \frac{6}{r^2} f_2(r)\right) + V_{20}(r) f_0(r) + V_{22}(r) f_2(r)$$

where

$$V_{00}(r) = V_{CT}(r) - 3V_{OPE}^{(2)}(r)$$

$$V_{20}(r) = V_{02}(r) = -6\sqrt{2} V_{OPE}^{(1)}(r)$$

$$V_{22}(r) = 6V_{OPE}^{(1)}(r) - 3V_{OPE}^{(2)}(r)$$

Computational Methods

The remaining matrix elements to compute are the $\mathbf{f_L}$ radial components.

$$\langle f_L(r) \mid \hat{T} + \hat{V} \mid f_L(r) \rangle$$

The potential energy components cannot be solved exactly, so we utilize the computational Gaussian-Laguerre quadrature integration technique. This method is similar to traditional trapezoidal Riemann sums but utilizes non-uniform intervals that are calculated and weighted to fit the Laguerre polynomials found within the integrand. Thus, the potential matrix elements' spatial integrals are computed directly, where $\boldsymbol{\omega_i}$ and $\mathbf{x_i}$ are the Gauss-Laguerre weights and points respectively.

$$\langle \nabla^{L',L} \rangle_{l',l} = \frac{N_{l'} N_l}{\gamma^3} \int_0^\infty dx \; x^2 e^{-x} L_{l'}^{(2)}(x) V_{L',L}(x/\gamma) L_l^{(2)}(x)$$

$$\simeq \frac{N_{l'} N_l}{\gamma^3} \sum_{i=1}^{N} \omega_i L_{l'}^{(2)}(x_i) V_{L',L}(x_i/\gamma) L_l^{(2)}(x_i)$$

Using the kinetic energy operator in spherical coordinates and performing the integral numerically, we find the kinetic energy components

$$\hat{T} = -\frac{1}{2\mu}\left(\frac{1}{r^2}\frac{\partial}{\partial r}\left(r^2 \frac{\partial}{\partial r}\right) + \frac{\hat{l}^2}{r^2}\right)$$

$$\langle \hat{T}^L \rangle_{l',l} = \frac{\hbar^2 \gamma^2}{2\mu}\left[(l + L(L+1)) I_{l',l}^{(2)} + (l+1) I_{l',l}^{(1)} - \sqrt{l(l+2)} I_{l',l-1}^{(2)} - \frac{1}{4}\delta_{l,l'}\right]$$

where $I^{(1)}$ and $I^{(2)}$ can be solved in terms of only l and l'

$$I_{l',l}^{(1)} = \frac{1}{2}\sqrt{\frac{(l+1)(l+2)}{(l'+1)(l'+2)}} \quad for \quad l \leq l'$$

$$I_{l',l}^{(2)} = \frac{1}{2}\sqrt{\frac{(l+1)(l+2)}{(l'+1)(l'+2)}}\left((l'+1) - \frac{l}{3}\right) \quad for \quad l \leq l'$$

Choosing to use the first 40 terms in the $\mathbf{f_L}$ expansion, our Hamiltonian becomes an 80x80 matrix after solving for these radial matrix elements. Once the Hamiltonian matrix is found, it can be plugged into the eigenvalue $\mathbf{c_l}$ the coefficients and energy.

Of interest is the Hamiltonian matrix itself, as shown in Fig. 3. The kinetic energy components have no cross-terms and are strongest in the D-wave (f⊠). Similarly, the pure spin/isospin components also lack cross-terms but are strongest in the S-wave (f_0) where they contribute a large attractive (negative) potential. Most interesting is the tensor components, which do have cross-terms, meaning there is interference happening between the S and D waves. This occurs due to the non-symmetric nature of the tensor operator as it couples the particles' spin and angular components. This tensor operator contributes additional attractive interactions between the proton and neutron and gives the deuteron some of its defining characteristics.

In addition to finding the Hamiltonian matrix, we can use the same Gauss-Laguerre quadrature integration to find various physical observables. In this particular study, we calculate the deuteron root-mean-square matter radius and the deuteron magnetic moment, given by the following operators:

- The rms matter radius where i is the index of the particle

$$\hat{r}^2 = \frac{1}{2}\sum_{i=1,2} r_i^2$$

- The magnetic moment

$$\hat{\mu}_z = \sum_{i=1,2}\left(\frac{1+\tau_z^i}{2}\right)\hat{l}_z^i + \sum_{i=1,2}\left[\mu_p\left(\frac{1+\tau_z^i}{2}\right) + \mu_n\left(\frac{1-\tau_z^i}{2}\right)\right]\sigma_z^i$$

Once the full wave function is known (having solved for the remaining $\mathbf{c_l}$ coefficients via the eigenvalue equation), Monte Carlo integration can be used as an alternative numerical method to calculate more complex operators. In this technique, the integral is approximated by the wave function's probability distribution, and the operator is calculated directly on the de-coupled neutron and proton particles.

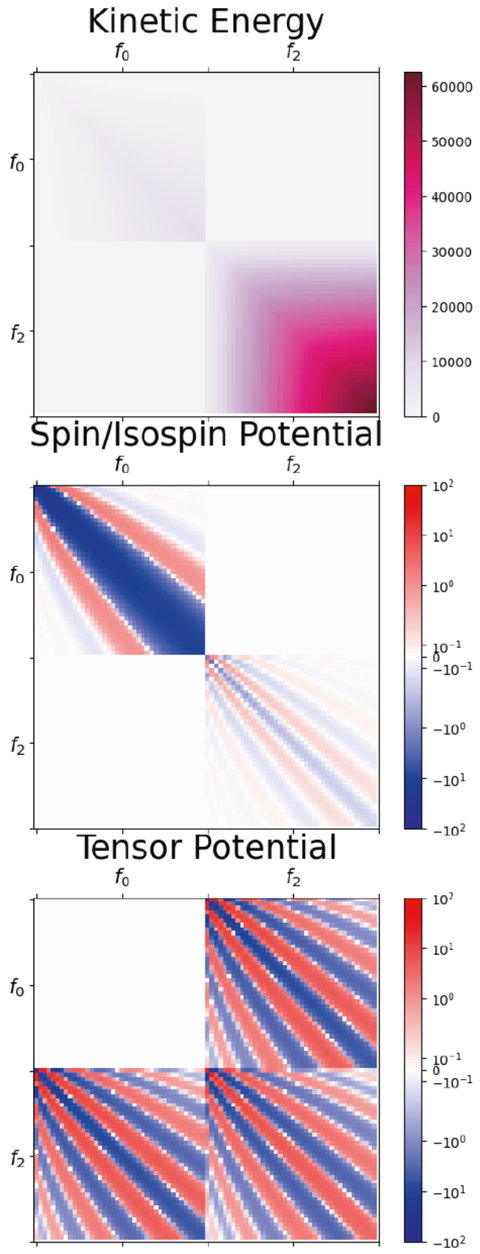

Figure 3: Full Hamiltonian matrix elements split into kinetic, pure spin/isospin, and tensor operator components, with f_0 and f_2 interaction terms on the off-diagonal quadrants and negative (blue) attractive potentials.

$$\langle \hat{O} \rangle = \frac{\langle \psi \mid \hat{O} \mid \psi \rangle}{\langle \psi | \psi \rangle} = \sum_{R_i \in P(r_1^i, r_2^i)} \frac{\psi_i^\dagger \hat{O} \psi_i}{|\psi_i|^2}$$

In this study, we use Monte Carlo integration to calculate the root-mean-squared matter radius as given previously. As this method relies on having a representative random sample, there is inherent √N error within the values measured. However, this error is inversely proportional to N where is the total sample size. Thus, it is important to use a large sample size (over 100,000 points) to produce a reasonable answer. This can be seen in Fig. 4 as the error bars decrease in size when the total sample size gets larger. Our final results are calculated using a total sample size of 300,000.

Results

From our analytic and computational solutions, we find the radial function expansion coefficients (c_1) and thus the radial functions themselves. A spatial plot of the f_0 and f_2 functions is shown in Fig. 5 as a function of relative distance between the two particles in the nucleus. Integrating over both waves, we find that the S-wave accounts for about 95.4% and the D-wave 4.6% of the deuteron ground state wave function. Both radial components approach zero at large and small r values, as expected from our construction of the expansion basis

Another set of results are the numerical values calculated for the deuteron binding energy, rms radius, and magnetic moment observables. The exact values are listed in Table 1. Additionally, experimental values are provided as a comparison to our theoretically derived numbers (Van Der Leun and Alderliesten, Mustafa, and Kellogg et al).

Table 1: Electromagnetic Observables

	Exact Numerical	Monte Carlo Numerical	Experimental
Binding Energy	$-2.2245\ MeV$	–	$-2.2246\ MeV$
RMS Matter Radius	$1.908\ fm$	$1.896 \pm 0.009\ fm$	$1.95\ fm$
Magnetic Moment	$0.8450\ \mu N$	–	$0.8574\ \mu N$

Finally, in order to ensure our Gauss-Laguerre quadrature integration is providing a stable answer, we perform the integration repeatedly, as shown in Fig. 6, while varying the algorithm parameters:

- M: The number of Laguerre Polynomials to include in the f_l expansion. Our final results were calculated using M = 40.
- N: The number of integration points in the quadrature integration. Our final results were calculated using N = 100.
- y: A parameter that controls the integration grid size when converting between integration points (x's) and physical distances (r's). Our final results are calculated using y = 4.0.

Discussion

Fig. 6 illustrates that the chosen algorithm parameters fall within the stable regions, where the calculated deuteron binding energy is not diverging. Thus, it is assumed that the numerical Gauss-Laguerre quadrature integration is accurate.

Additionally, we have strong agreement within 1 percent between the theoretically calculated and experimentally found observable values. As they match closely, we can conclude the low energy model used to derive the results is an accurate representation of the ground state deuteron nucleus.

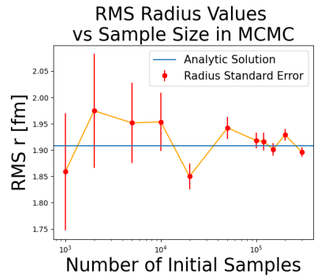

Figure 4: Root-mean-squared matter radius values for varying sample sizes in Markov Chain Monte Carlo integration, showing the reduction in error as sample size grows.

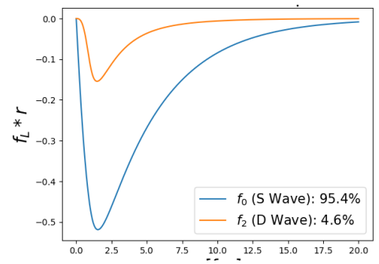

Figure 5: The radial wave function components with c_L coefficients solved as a function of distance. Both the S (L=0) and D (L=2) waves are negative (attractive) at close range and go to zero at large r values.

A further conclusion is that the first order interaction potential defined at the start of this paper is valid under the low energy assumptions (where the proton/neutron internal structures are negligible).

The next steps for this project are to calculate more observables using the Monte Carlo integration, including electron-deuteron elastic scattering form factors and cross sections. These values could then be compared to Jefferson Laboratory scattering data, further constraining the theoretical model.

About the Author

Sarah Heller is a senior at Montana State University majoring in Physics and Mathematics, with a minor in data science. During the summer of 2025, she conducted theoretical nuclear physics research at the Thomas Jefferson National Accelerator Facility in Virginia. Sarah plans to pursue a PhD in particle physics, studying neutrinos or high energy collider physics. She has served as an officer of the Society of Physics Students club and worked as a tutor at the Math and Stat Center since 2022. Outside of academics, Sarah enjoys dancing, reading science fiction, and drinking tea.

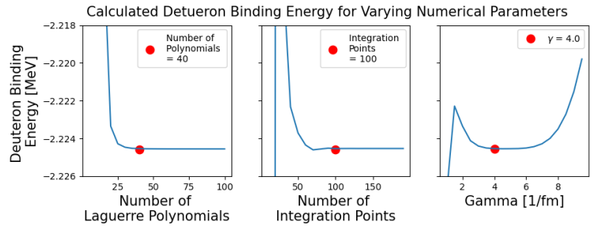

Figure 6: To validate the Gaussian-Laguerre quadrature integration, we vary the numerical parameters and plot the calculated ground-state energy to show they produce a stable value.

Acknowledgements

This material is based upon work supported by the National Science Foundation under Grant #2348822.

References

Kellogg, J. M., Rabi, I. I., Ramsey, N. F., & Zacharias, J. R. (1940). An electrical quadrupole moment of the deuteron the radiofrequency spectra of HD and. Physical Review, 57(8), 677–695. https://doi.org/10.1103/physrev.57.677

Mustafa, M. M. (1993). Radius and radial moments of the Deuteron. Physical Review C, 48(2), 929–932. https://doi.org/10.1103/physrevc.48.929

Piarulli, M., Girlanda, L., Schiavilla, R., Pérez, R. N., Amaro, J. E., & Arriola, E. R. (2015). Minimally nonlocal nucleon-nucleon potentials with chiral two-pion exchange including. Physical Review C, 91(2). https://doi.org/10.1103/physrevc.91.024003

Van Der Leun, C., & Alderliesten, C. (1982). The Deuteron Binding Energy. Nuclear Physics A, 380(2), 261–269. https://doi.org/10.1016/0375-9474(82)90105-1

van Kolck, U. (2020). The problem of renormalization of chiral nuclear forces. Frontiers in Physics, 8. https://doi.org/10.3389/fphy.2020.00079

DOI https://doi.org/10.15788/739245823